ORIGINAL ARTICLE

lajss.org© Latin American Journal of Solids and Structures

www.lajss.org

A physics-based fast algorithm for structural responses of generalized rotationally axisymmetric structures: the generalized rotation-superposition method

Mao Yang[a], Jun Zhang[a], Hao Chen[a], Jialin Yang[a], Yongjian Mao[a]*

[a]Institute of Systems Engineering, China Academy of Engineering Physics, Mianyang 621999, Sichuan, PR China.
Email: lxym93@caep.cn, hjzhangj@caep.cn, chenhao211@gscaep.ac.cn, yangjialin22@gscaep.ac.cn, maoyj@caep.cn

*Corresponding author

https://doi.org/10.1590/1679-78257938

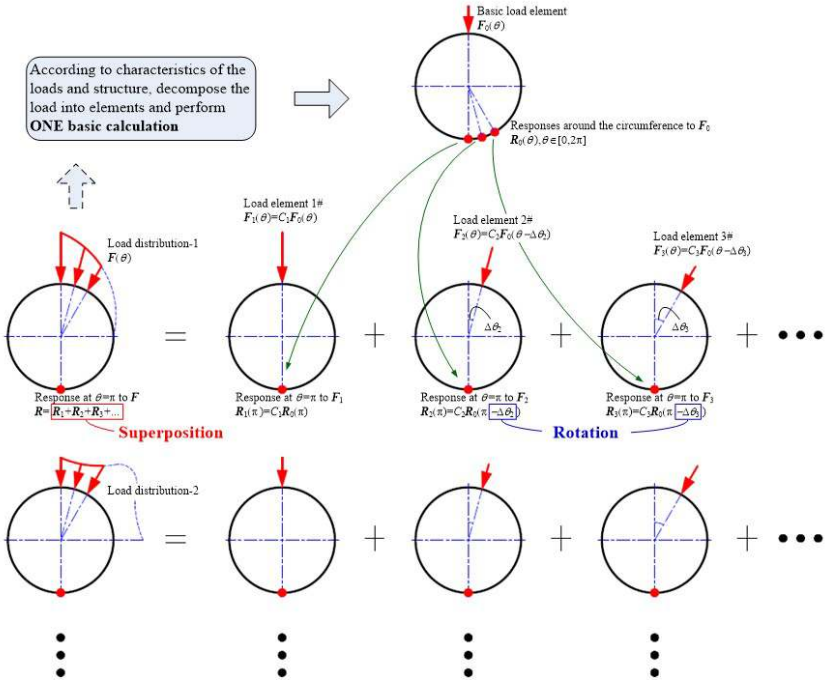
Abstract

Fast calculations are widely required in the traditional applications and the emerging digital twin fields. For those considerations, a novel physics-based fast algorithm, namely generalized rotation-superposition method, is proposed for fast calculating linear elastic responses of generalized rotationally axisymmetric structures under arbitrary mechanical loads. This improved method breaks through the limitations of the previous basic rotation-superposition method in rotational similarity of load and structural axisymmetry, and greatly expands its application scope. In this paper, firstly, the basic theory of the rotation-superposition algorithm is introduced; secondly, the theoretical model of the generalized rotation-superposition method is established; thirdly, the effectiveness and accuracy are verified by using finite element simulations; finally, through a complex case study, the applicability of the generalized rotation-superposition method for complex engineering problems and its advantages in efficiently obtaining massive amounts of data are further illustrated.

Keywords

fast algorithm; structural response; axisymmetric structure; rotationally axisymmetric structure; rotation-superposition method; digital twin

Graphical Abstract



Received: November 16, 2023. In revised form: April 07, 2024. Accepted: April 23, 2024. Available online: April 26, 2024.
https://doi.org/https://doi.org/10.1590/1679-78257938

Latin American Journal of Solids and Structures. ISSN 1679-7825. Copyright © 2024. This is an Open Access article distributed under the terms of the Creative Commons Attribution License, which permits unrestricted use, distribution, and reproduction in any medium, provided the original work is properly cited.

1 INTRODUCTION

Fast calculations are one aspect of the goals continually pursued in computational mechanics, structural mechanics, and the related engineering fields. It is well known that the traditional requirements of fast structural analysis involve sensitivity analysis, optimization design, reliability assessment, uncertainty quantification, and so on. Meanwhile, a newly emerging and promising technology, the digital twin (Laplante 2022), is gradually accelerating its development and broadening its applications. In many occasions, structural digital twin technology requires fast, even real-time structural calculations for online monitoring, analyzing, and predicting the structural status or performance (Guo, Zhuang, and Rabczuk 2019; Lai et al 2022; He et al 2022). Therefore, the driving power of development of fast structural computations is much stronger than ever before.

The methods for structural response computations could be divided into three categories as follows according to their different features and uses.

The first category is analytical method. Comparatively, analytical solutions can only be achieved for problems of simple structures, simple boundaries, and simple loads, although the precision and efficiency are relatively high.

The second category is numerical simulation (Ismail et al 2013; Ismail et al 2015; Ismail et al 2020; Yang et al 2021b; Kudela and Matousek 2022; Addisu and Koricho 2022; Feng, Zhang, and Khandelwal 2022; Lai et al 2022; He et al 2022; Norman et al 2023; Koocheki and Pietruszczak 2023; Lai et al 2023). Most numerical structural simulation methods, including the most well-known finite element method, are based on discretization and approximation of differential equations of continuous problems. Those methods have high applicability for structural complexity, high precision, and low efficiency. In addition, there are various new computational approaches based on deep neural networks (DNN) (Guo, Zhuang, and Rabczuk 2019; Samaniego et al 2020; Zhuang et al 2021) with the features of high efficiency, high precision and relatively low applicability for structural complexity, which are similar to the conventional analytical methods and can be regarded as semi-analytical or hybrid methods.

The third category is surrogate model (Alizadeh, Allen, and Mistree 2020; Yang et al 2021b; Kudela and Matousek 2022; Lai et al 2023). Currently, the method of surrogate model is a research hotspot in various fields. It is based on limited or finite data, usually obtained by calculations, experiments, or online monitoring, to build correlations among the related parameters to approximately represent the original high-complexity and large-scale problems of computational mechanics. Surrogate models include the response surface method (RSM) model (Yang et al 2021b; Kabasi, Roy, and Chakraborty 2021; Addisu and Koricho 2022; Yang et al 2023), artificial neural network (ANN) model (Stoffel et al 2020; Wang et al 2020; Guo and Wang 2020; Guo et al 2022; Koocheki and Pietruszczak 2023) and DNN model (Feng, Zhang, and Khandelwal 2022; Hu et al 2022), radial basis function (RBF) model (Stoffel et al 2020; Wang et al 2020; Chen et al 2022; Santana et al 2023), Kriging model (Jin and Jung 2016; Feng et al 2022; Wang et al 2023; Pang et al 2023), support vector regression (SVR) model (Keshtegar et al 2021; Mahmoodzadeh et al 2022; Funk, Basmaji, and Nackenhorst 2023; Zhou and Peng 2023) and moving-least-squares method (MLSM) model (Kabasi, Roy, and Chakraborty 2021; Teng, Feng, and Chen 2022), and so on. There are several approaches for building surrogate models, such as curve/surface fitting or regression (He et al 2022; Yang et al 2021b; Addisu and Koricho 2022; Kabasi, Roy, and Chakraborty 2021; Guo et al 2022; Keshtegar et al 2021; Mahmoodzadeh et al 2022; Funk, Basmaji, and Nackenhorst 2023; Zhou and Peng 2023; Yang et al 2023), and machine learning (Samaniego et al 2020; Guo and Wang 2020; Zhuang et al 2021; Feng et al 2022; Wang et al 2023; Zhou and Peng 2023). Essentially, the method of surrogate model is data-driving, entirely different from the above two categories of physics-based methods, i.e. analytical and numerical methods. Comparatively, this method has high efficiency and high applicability for structural complexity, but low precision. The features of the above three categories of structural analysis methods can be illustrated as Figure 1(a). Due to their different advantages and disadvantages, the three methods play different roles in engineering and scientific applications. For fast computations, especially in emerging digital twin applications, surrogate models have an absolute dominance because of their high efficiencies although they have relatively low precision.

Combinations of numerical simulations and surrogate models can make the best use of their advantages and bypass their disadvantages, and significantly obtain a balance between precision and efficiency, as shown in Figure 1(b). This kind of approaches have already been studied and used by a number of researchers. Kudela and Matousek (2022) reviewed 180 significant publications referring to surrogate modeling for finite element method-based computations, and expected to concentrate on decreasing computational cost related to deriving surrogate models. Yang et al (2021b), Addisu and Koricho (2022) accomplished a multi-objective optimization by building response surface models based on finite element results. Feng, Zhang, and Khandelwal (2022), Koocheki and Pietruszczak (2023) performed multiscale finite simulations with data-driven homogenization constitutive models using artificial neural networks and deep neural networks, respectively, which were trained by previous meso scale finite element calculations. Lai et al (2022, 2023) and

He et al (2022) studied the digital twin frameworks where the surrogate models were fed by structural results by finite element simulations, and improved the real-time monitoring and prediction accuracy of the structural performances.

However, sometimes, there is a conflict between the amount of data requirements and the feeding capacity of numerical simulations due to the low efficiencies for complex structures. The precision and reliability of the surrogate models are unavoidably affected by the quantities and qualities of supplied samples. This just explains why Kudela and Matousek (2022) proposed to decrease computational cost in deriving surrogate models, why Lai et al (2022) built high- and low-fidelity finite element models to feed the multifidelity surrogate model to improve the real-time monitoring and prediction accuracy of the structural safety, and why Lai et al (2023) developed a node rearrangement method in finite element modeling to improve the ability of digital twin to mirror the entire complex structure and balance the computational cost and accuracy. Thus, it can be found that there is a development potential, to find an enhancer as shown in Figure 1(c), helping finite element simulations to improve data supplying efficiencies, and then improve the final precisions by supplying more data for regression or training.

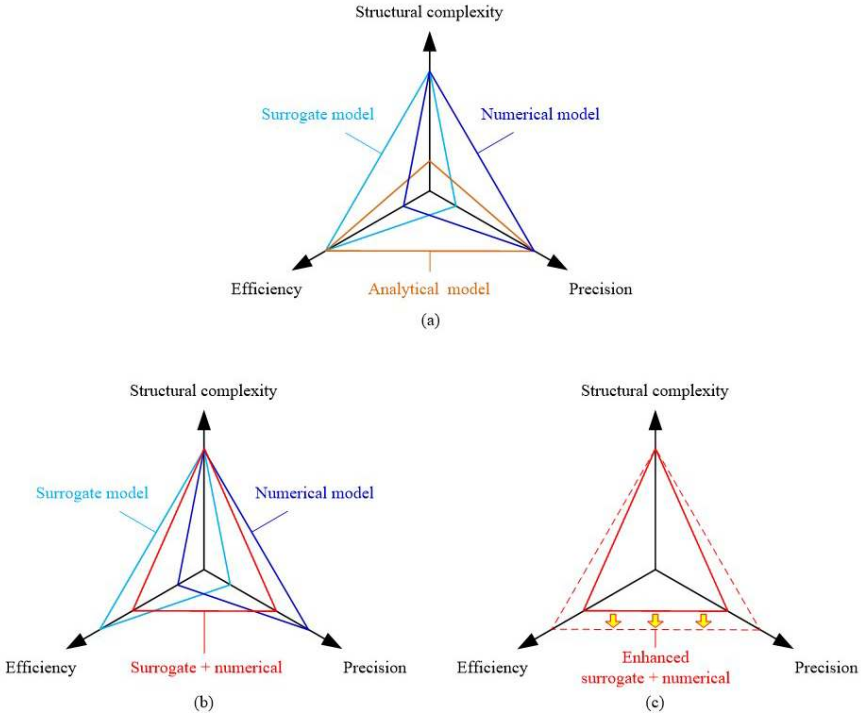


Figure 1. Three categories of structural computation models. (a) features of the three models; (b) features of combinations of surrogate models and numerical models; (c) development potential of enhanced combinations of surrogate models and numerical models.

This study just aims at this growth point and focuses on a novel fast method as an enhancer for data supplying from numerical simulations to surrogate models which is necessary for further improvement of the computation efficiencies and precision in a specific class of structural digital twin applications. The early idea of the method was proposed by Mao et al (2010) for calculating the lateral shock responses of axisymmetric structures. The algorithm only needs to calculate the response of a load element, and then can change various load parameters (such as spatial distribution parameters and time synchronization parameters), obtain the corresponding structural responses by coordinate rotation and linear superposition, and then obtain the variation law of structural responses to related parameters. The algorithm only involves arithmetic operations, which are much faster than numerical methods such as the finite element method, and is especially suitable for the rapid analysis of a large number of working conditions. In 2011, the algorithm was extended to solve the elastic responses of axisymmetric structures subjected to rotationally similar loads, and was named as “rotation-superposition method” (Mao et al 2011a). The rotationally similar load mentioned above is defined as a load that can be divided into a number of load elements, and each element can be rotated by an appropriate angle to be similar (proportional) to the native element. Subsequently, it was applied to solve the problem of pyroshock responses induced by the pyrotechnical separation of aerospace structures (Mao et al 2011b). Based on the structural response analysis of a single explosion bolt (as a basic load element), the structural responses under different numbers, distribution positions, and initiation times of explosion bolts were obtained by using the rotation-superposition method. Furthermore, this method was also used to analyze the responses of cylindrical and conical shells subjected to explosive rods to simulate the

corresponding loads induced by intense pulsed X-ray blow-off (Mao et al 2019). Based on the calculation results of the shock responses to a single explosive rod (as a basic load element), combined with enumerated envelope analysis and Monte Carlo sampling analysis, and changing the parameters such as the number, distribution parameters, and initiation time delays of the explosive rods, a large number of calculations referring to more than 100,000 working conditions were performed while obtaining the influence law of each parameter on the structural responses. This application sufficiently demonstrated the efficiency and superiority of this algorithm in fast batch solutions.

From the above introduction, it can be seen that the rotation-superposition method is a novel fast algorithm that differs from the above three categories of structural response computation methods. The most significant characteristic is physics-based rather than data-driving. It is completely faithful to the original physics-based models because it is derived by the principle of superposition, one of the most classical principles in the theory of elasticity (Tiemoshenko and Goodier 2004), and the basic results used for superposition are calculated by physics-based numerical methods such as the finite element method. The second characteristic is high-efficiency because it only arithmetically combines the basic calculation results into a large number of results with different parameters, which basically does not sacrifice accuracy and has a very high cost-effectiveness ratio.

However, the application scope of the above rotation-superposition method is limited to a certain extent, that is: 1) the load must be rotationally similar; and 2) the structure must be axisymmetric. Thus, in this study, the method described by Mao et al (2011a) is greatly improved and expanded, by breaking through the two limitations of rotational similarity of load and structural axisymmetry, and forming a more general and systematic algorithm system suitable for arbitrary mechanical loads and generalized rotationally axisymmetric structures (including axisymmetric structures and periodically axisymmetric structures). This method provides an efficient and precise batch analysis method for structural response calculations in both emerging digital twin techniques and traditional applications such as sensitivity analysis, optimization design, reliability assessment, and uncertainty quantification.

The remainder of this paper is organized as follows. In Section 2, the early basic theory of rotation-superposition method is introduced, and based on that, the generalized rotation-superposition method is derived; in Section 3, the newly extended method is verified by finite element simulations; in Section 4, a complex application is given and the results are discussed; and in Section 5, the final conclusions, as well as a note about future work are contained. The flowchart of the research is shown in Figure 2.

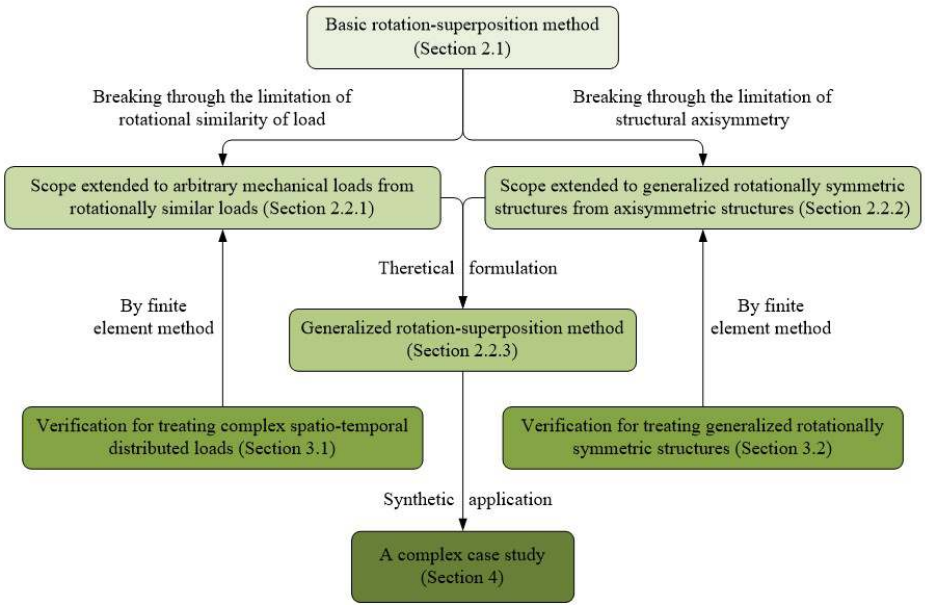


Figure 2. The flowchart of the research.

2 THEORY

2.1 Basic theory of rotation-superposition method

2.1.1 Theory

According to previous studies (Mao et al 2011a; Mao et al 2011b; Mao et al 2019), the basic theory of the rotation-superposition method can be briefly described as follows.

Assuming an axisymmetric body V, subjected to load $\boldsymbol{F}(r,\theta,z,t)$ at point set $\Omega(r,\theta,z,t) \subseteq V$, now we decompose $\boldsymbol{F}$ in some way:

$$\boldsymbol{F}(r,\theta,z,t)=\sum_{i=1}^{n}\boldsymbol{F}_i(r,\theta,z,t),\ \ n\geqslant 1 \tag{1}$$

where r, θ and z are cylindrical coordinates, t is the time, n is the number of load elements, and $\boldsymbol{F}_i$ is the ith load element. If $\Omega_i(r,\theta,z,t) \subseteq \Omega$ is the loading point set (which may be points, areas, or volumes) of load element $\boldsymbol{F}_i$ and satisfies:

$$\Omega_i(r,\theta-\Delta\theta_i,z)=\Omega_1(r,\theta,z),\ \ i=1,2,\cdots,n \tag{2}$$

and there is a proportional relationship:

$$\boldsymbol{F}_i(r,\theta-\Delta\theta_i,z,t-\Delta t_i)=C_i\boldsymbol{F}_0(r,\theta,z,t),\quad i=1,2,\cdots,n \tag{3}$$

where $\boldsymbol{F}_0(r,\theta,z,t)$ denotes a basic load element, it can be said that load $\boldsymbol{F}$ on the axisymmetric body V has rotational similarity, or load $\boldsymbol{F}$ is a rotationally similar load. In other words, a rotationally similar load is defined as a load that can be divided into a number of load elements and each element can be rotated by an appropriate angle to be similar (proportional) to the native element.

In this case, the response of the structure under the load $\boldsymbol{F}_i$ is defined as:

$$\boldsymbol{R}_i=\boldsymbol{R}_i\left(r,\theta,z,t\right),\ \ i=0,1,2,\cdots,n \tag{4}$$

where $\boldsymbol{R}_i$ represents the component of the structural response under load $\boldsymbol{F}_i$ in a cylindrical coordinate system. Assuming that the response under basic load element $\boldsymbol{F}_0$ is $\boldsymbol{R_0} = \boldsymbol{R_0}(r,\theta,z,t)$, the response under load element $\boldsymbol{F}_i$ can be obtained by the linear assumption as follows:

$$\boldsymbol{R}_i\left(r,\theta,z,t\right)=C_i\boldsymbol{R}_0\left(r,\theta-\Delta\theta_i,z,t-\Delta t_i\right),\quad i=1,2,\cdots,n \tag{5}$$

where C_i is the ith load factor, which is determined using equation (3).

According to the principle of superposition in the theory of elasticity, the total response is the linear superposition of the responses under all load elements, i.e.:

$$\boldsymbol{R}\left(r,\theta,z,t\right)=\sum_{i=1}^{n}\boldsymbol{R}_i\left(r,\theta,z,t\right)=\sum_{i=1}^{n}C_i\boldsymbol{R}_0\left(r,\theta-\Delta\theta_i,z,t-\Delta t_i\right) \tag{6}$$

The above is the basic theory of the rotation-superposition method. An illustration of this method is shown in Figure 3. It can be observed that the method can obtain many results under different load distributions (Load distribution-1, Load distribution-2, ...) based on only one basic numerical calculation (Responses $\boldsymbol{R}_0$ to basic load element $\boldsymbol{F}_0$).

2.1.2 Limitations

The derivation of the above rotation-superposition method is based on some certain assumptions, and its applicable scope is limited as follows.

- Rotationally similar loads. The load must have a property of rotational similarity, as shown in equation (3), and its specific connotation includes two aspects: 1) the spatial distribution is similar, that is, the amplitude distribution at the corresponding points of different load elements is proportional, and 2) the time domain distribution is the same, that is, the load time histories at the corresponding points of different load elements are the same after normalization.
- Axisymmetric structures. The structure must be an axisymmetric body such as a cylinder or cone.
- Linear problems. The material is in the stage of linear elasticity, and it does not involve other nonlinear factors such as large geometric deformation, hyperelastic deformation, plastic deformation, and contact friction.
- Vector responses. The response calculated by the rotation-superposition method must be a vector in a cylindrical coordinate system, such as displacement, velocity, acceleration, stress, and strain.

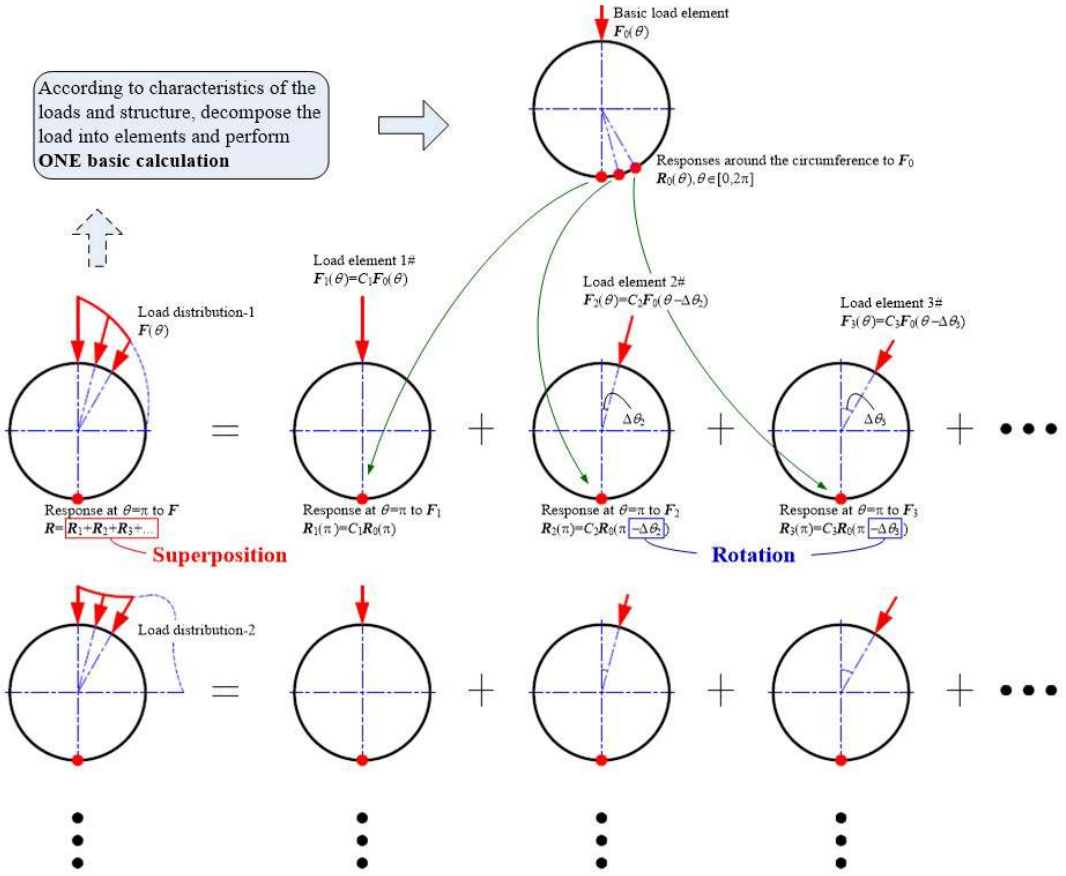


Figure 3. Illustration of the basic theory of rotation-superposition method.

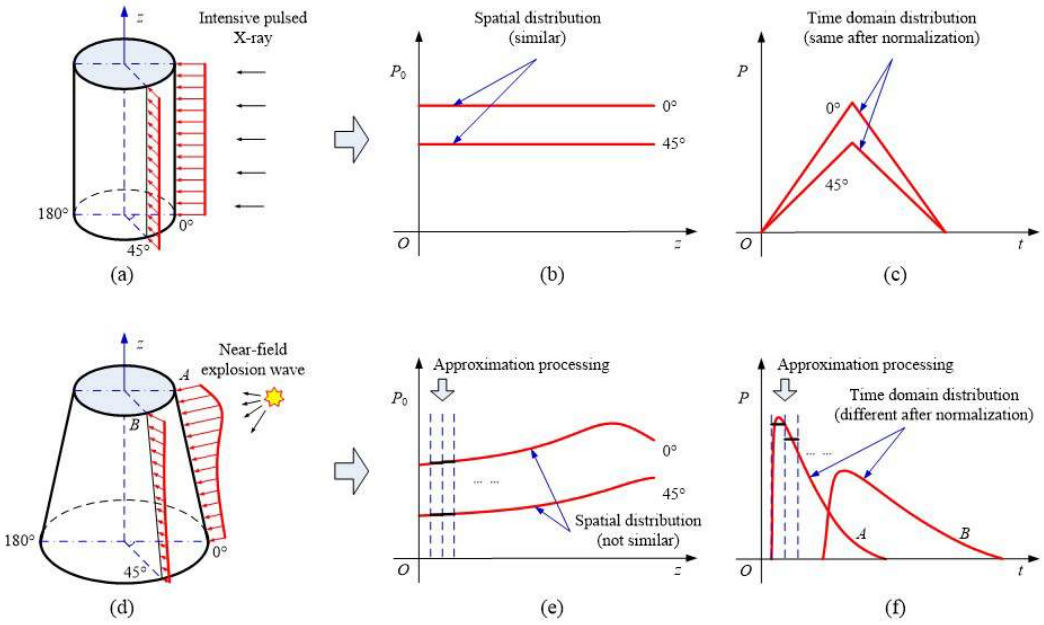


Figure 4. Typical loads with rotational similarity or not. (a) load model of cylindrical shell subjected to a transient pressure load induced by intense pulsed X-ray; (b) spatial distribution of the X-ray load; (c) temporal distribution of the X-ray load; (d) load model of conical shell subjected to a near-field blast load; (e) spatial distribution and its approximation of the blast load; (f) temporal distribution and its approximation of the blast load.

2.2 Derivation of generalized rotation-superposition method

Owning to the above assumptions and limitations, the requirements of the rotational similarity of load and axisymmetry of structures have considerable restrictions on the popularization and application of the method. To overcome these limitations, this study established a theory of the generalized rotation-superposition method.

2.2.1 Treatment and formulation for complex spatio-temporal distributed loads

According to equation (3), the rotational similarity of load requires similar spatial distributions and time-domain distributions, as shown in Figures 4(a), (b), and (c), where the cylindrical shells are subjected to a transient pressure load induced by an intense pulsed X-ray. However, in reality, many loads have different spatial and temporal distributions at different positions, which cannot meet or completely meet the above conditions. For example, for a conical shell subjected to a near-field explosion, the load pulse duration near the explosion point is short and the amplitude is high, whereas the load pulse duration far from the explosion point is long and the amplitude is low; that is, the spatial distribution and time-domain distribution of the loads are different at different points, thus there is not rotational similarity, as shown in Figures 4(d), (e), and (f).

To solve the problem of dissimilar spatial distribution of load, the load can be divided into several sections along the axial direction, and the amplitude of the load in each section can be approximately replaced by its average value; thus, the load in each section approximately satisfies the condition of similar spatial distribution, as shown in Figure 4(e). Assuming that the load is divided into m sections along the axis direction, equation (3) becomes:

$$\boldsymbol{F}_{ij}(r,\theta-\Delta\theta_{ij},z,t-\Delta t_{ij})=C_{ij}\boldsymbol{F}_{0j}(r,\theta,z,t),\quad i=1,2,\cdots,n;\ j=1,2,\cdots,m \tag{7}$$

Equation (4) becomes:

$$\boldsymbol{R}_{ij}=\boldsymbol{R}_{ij}\left(r,\theta,z,t\right),\quad i=0,1,2,\cdots,n;\ j=1,2,\cdots,m \tag{8}$$

Equation (5) becomes:

$$\boldsymbol{R}_{ij}\left(r,\theta,z,t\right)=C_{ij}\boldsymbol{R}_{0j}\left(r,\theta-\Delta\theta_{ij},z,t-\Delta t_{ij}\right),\quad i=1,2,\cdots,n;\ j=1,2,\cdots,m \tag{9}$$

Equation (6) becomes:

$$\boldsymbol{R}\left(r,\theta,z,t\right)=\sum_{i=1}^{n}\sum_{j=1}^{m}\boldsymbol{R}_{ij}\left(r,\theta,z,t\right)=\sum_{i=1}^{n}\sum_{j=1}^{m}C_{ij}\boldsymbol{R}_{0j}\left(r,\theta-\Delta\theta_{ij},z,t-\Delta t_{ij}\right) \tag{10}$$

To address the problem of varying load distributions in the time domain, referring to the Duhamel Integral (Nakamura 2012), the load can be divided into several segments in the time domain, and each segment can be replaced by a rectangular distributed load. Thus, the entire time history curve can be obtained by the amplitude scaling and time-domain combination of a basic short-time rectangular distributed load, as shown in Figure 4(f). Assuming that the load is divided into l segments in the time domain, equation (3) becomes:

$$\boldsymbol{F}_{ik}(r,\theta-\Delta\theta_{i},z,t-\Delta t_{ik})=C_{ik}\boldsymbol{F}_{0k}(r,\theta,z,t),\quad i=1,2,\cdots,n;k=1,2,\cdots,l \tag{11}$$

Equation (4) becomes:

$$\boldsymbol{R}_{ik}=\boldsymbol{R}_{ik}\left(r,\theta,z,t\right),\quad i=0,1,2,\cdots,n;k=1,2,\cdots,l \tag{12}$$

Equation (5) becomes:

$$\boldsymbol{R}_{ik}\left(r,\theta,z,t\right)=C_{ik}\boldsymbol{R}_{0k}\left(r,\theta-\Delta\theta_{i},z,t-\Delta t_{ik}\right),\quad i=1,2,\cdots,n;k=1,2,\cdots,l \tag{13}$$

Equation (6) becomes:

$$\boldsymbol{R}\left(r,\theta,z,t\right)=\sum_{i=1}^{n}\sum_{k=1}^{l}\boldsymbol{R}_{ik}\left(r,\theta,z,t\right)=\sum_{i=1}^{n}\sum_{k=1}^{l}C_{ik}\boldsymbol{R}_{0k}\left(r,\theta-\Delta\theta_{i},z,t-\Delta t_{ik}\right) \tag{14}$$

Methods similar to those proposed above can be used for problems with complex spatio-temporal distributions of loads. Assuming that the load is divided into m sections along the axis direction and simultaneously divided into l segments in the time domain, equation (3) becomes

$$\boldsymbol{F}_{ijk}(r,\theta-\Delta\theta_{ij},z,t-\Delta t_{ijk})=C_{ijk}\boldsymbol{F}_{0jk}(r,\theta,z,t),\quad i=1,2,\cdots,n;j=1,2,\cdots,m;k=1,2,\cdots,l \tag{15}$$

Equation (4) becomes:

$$\boldsymbol{R}_{ijk}=\boldsymbol{R}_{ijk}\left(r,\theta,z,t\right),\quad i=0,1,2,\cdots,n;j=1,2,\cdots,m;k=1,2,\cdots,l \tag{16}$$

Equation (5) becomes:

$$\boldsymbol{R}_{ijk}\left(r,\theta,z,t\right)=C_{ijk}\boldsymbol{R}_{0jk}\left(r,\theta-\Delta\theta_{ij},z,t-\Delta t_{ijk}\right),\quad i=1,2,\cdots,n;j=1,2,\cdots,m;k=1,2,\cdots,l \tag{17}$$

Equation (6) becomes:

$$\boldsymbol{R}\left(r,\theta,z,t\right)=\sum_{i=1}^{n}\sum_{j=1}^{m}\sum_{k=1}^{l}\boldsymbol{R}_{ijk}\left(r,\theta,z,t\right)=\sum_{i=1}^{n}\sum_{j=1}^{m}\sum_{k=1}^{l}C_{ijk}\boldsymbol{R}_{0jk}\left(r,\theta-\Delta\theta_{ij},z,t-\Delta t_{ijk}\right) \tag{18}$$

Then, using the treatment methods proposed above, the problems with complex spatio-temporal load distributions, that is, arbitrary loads, can be solved well. Therefore, the limitation of rotationally similar loads in the early rotation-superposition method has been successfully overcome.

2.2.2 Treatment and formulation for generalized rotationally symmetric structures

According to the basic theory of the rotation-superposition method presented in Section 2.1, the structure must be axisymmetric. Here, we expand the applicable scope of the structure style to include rotationally axisymmetric structures and provide a generalized expression.

Rotationally axisymmetric structures, also known as periodically axisymmetric structures, are structures that completely coincide with themselves after rotating by any integer multiple of a certain angle around a certain axis. This type of structures are widely used in engineering, such as rotors of aero-engines, hydraulic turbines, fans and other rotating mechanisms, various gears, and composite or sandwich shells (Ismail et al 2013; Ismail et al 2015; Yang et al 2021a; Yang et al 2022). Assuming that the axisymmetric period is θ_0, as shown in Figure 5, it is a rotationally axisymmetric structure when $\theta_0 > 0$ whereas it is an axisymmetric structure when $\theta_0 = 0$. Thus, the two types of structures can be uniformly expressed as “generalized rotationally axisymmetric structures”.

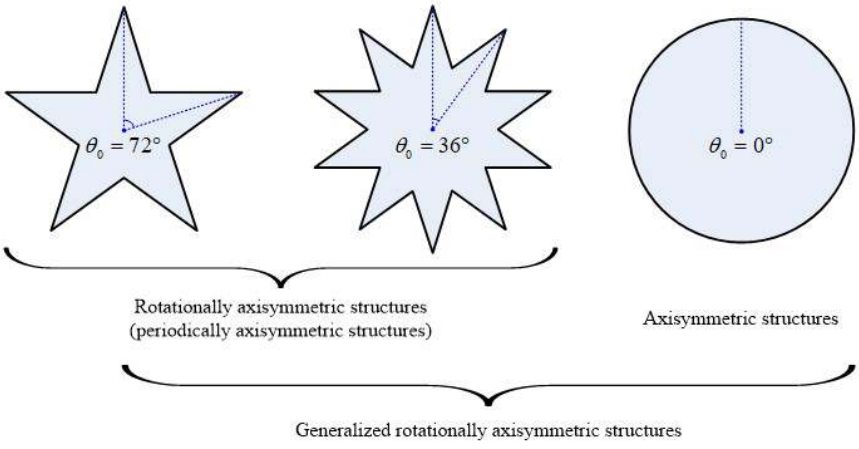


Figure 5. Cross sections of generalized rotationally axisymmetric structures.

According to the basic theory of the rotation-superposition method, for axisymmetric structures, both the load elements and the corresponding responses can be superimposed by rotating by a certain angle $\Delta\theta$. However, for rotationally axisymmetric structures, because of the existence of the axisymmetric period θ_0, the rotation-superposition method can only rotate by an integer multiple of θ_0. Otherwise, the corresponding relationship between the load and the structure will change, and the condition of the rotation-superposition method will no longer be met. Therefore, to improve the basic theory of the rotation-superposition method and make it applicable to generalized rotationally axisymmetric structures, it is only necessary to specify that the rotational angle is an integer multiple of the axisymmetric period, that is, $\Delta\theta = s\theta_0$, where s is an integer. When the symmetry period is equal to zero, that is, $\theta_0 = 0$, as shown in Figure 5, the rotationally axisymmetric structure degenerates into an axisymmetric structure. It then regresses to the

previous basic theory, and there is no restriction on $\Delta\theta$. Thus, for axisymmetric and rotationally axisymmetric structures, uniformly named generalized rotationally axisymmetric structures, the theory of the rotation-superposition method can be also generalized.

2.2.3 Formulation of generalized rotation-superposition method

According to the above treatment methods, the generalized rotation-superposition method for generalized rotationally axisymmetric structures under complex spatio-temporal distributed loads can be established.

Assume a rotationally axisymmetric structure V, whose axisymmetric period is θ_0, subjected to load $\boldsymbol{F}(r,\theta,z,t)$ at point set $\Omega(r,\theta,z,t) \subseteq V$. Decompose $\boldsymbol{F}$ in some way:

$$\boldsymbol{F}(r,\theta,z,t)=\sum_{i=1}^{n}\sum_{j=1}^{m}\sum_{k=1}^{l}\boldsymbol{F}_{ijk}(r,\theta,z,t) \quad n\geqslant 1, m\geqslant 1, l\geqslant 1 \tag{19}$$

where n denotes the number of load elements, m denotes the number of axial load sections, l denotes the number of time-domain load segments, and $\boldsymbol{F}_{ijk}$ denotes the load element. If $\Omega_{ij}(r,\theta,z) \subseteq \Omega$ is the loading point set of element $\boldsymbol{F}_{ijk}$, it can be decomposed to satisfy:

$$\Omega_{ij}(r,\theta-\Delta\theta_{ij},z)=\Omega_{1j}(r,\theta,z) \quad i=1,2,\cdots,n;\ j=1,2,\cdots,m \tag{20}$$

$$\Delta\theta_{ij}=\begin{cases} s\theta_0, & \theta_0\neq 0, s=1,2,\cdots \\ \text{a nonzero real number}, & \theta_0=0 \end{cases} \tag{21}$$

$$\boldsymbol{F}_{ijk}(r,\theta-\Delta\theta_{ij},z,t-\Delta t_{ijk})=C_{ijk}\boldsymbol{F}_{0jk}(r,\theta,z,t) \quad i=1,2,\cdots,n;\ j=1,2,\cdots,m;\ k=1,2,\cdots,l \tag{22}$$

where $\boldsymbol{F}_{0jk}(r,\theta,z,t)$ is the basic load element. The above equations show that the load $\boldsymbol{F}$ on the rotationally axisymmetric structure V is divided into l segments in the time domain and m sections in the space domain, and that the load subset $\boldsymbol{F}_{ijk}$ formed by the above method has rotational similarity.

In this case, the response of the structure under load $\boldsymbol{F}_{ijk}$ is:

$$\boldsymbol{R}_{ijk}=\boldsymbol{R}_{ijk}\left(r,\theta,z,t\right), \quad i=0,1,\cdots,n;\ j=1,2,\cdots,m;\ k=1,2,\cdots,l \tag{23}$$

Where $\boldsymbol{R}_{ijk}$ represents the component of the structural response under load element $\boldsymbol{F}_{ijk}$ in the cylindrical coordinate system.

Assuming that $\boldsymbol{R}_{0jk}=\boldsymbol{R}_{0jk}(r,\theta,z,t)$ is the response under the basic load element $\boldsymbol{F}_{0jk}$, the response under load element $\boldsymbol{F}_{ijk}$ can be obtained by the linear assumption as follows:

$$\boldsymbol{R}_{ijk}\left(r,\theta,z,t\right)=C_{ijk}\boldsymbol{R}_{0jk}\left(r,\theta-\Delta\theta_{ij},z,t-\Delta t_{ijk}\right), \quad i=1,2,\cdots,n;\ j=1,2,\cdots,m;\ k=1,2,\cdots,l \tag{24}$$

where C_{ijk} is the load factor determined using equation (22).

According to the principle of superposition, the total response is the linear superposition of the responses under the $n\times m\times l$ load elements:

$$\boldsymbol{R}\left(r,\theta,z,t\right)=\sum_{i=1}^{n}\sum_{j=1}^{m}\sum_{k=1}^{l}\boldsymbol{R}_{ijk}\left(r,\theta,z,t\right)=\sum_{i=1}^{n}\sum_{j=1}^{m}\sum_{k=1}^{l}C_{ijk}\boldsymbol{R}_{0jk}\left(r,\theta-\Delta\theta_{ij},z,t-\Delta t_{ijk}\right) \tag{25}$$

Equation (25) is a unified expression for the generalized rotation-superposition method. When $m=1$, it degenerates into the axial non-section of load; when $l=1$, into the time-domain non-segmentation of load; when $\theta_0=0$, into the axisymmetric structure; and when $m=1$, $l=1$ and $\theta_0=0$, it completely degenerates into the previous basic rotation-superposition method.

3 VERIFICATION

3.1 For complex spatio-temporal distributed loads

3.1.1 Problem description

Assuming that the outer surface of the cylindrical shell is subjected to a dynamic surface load, the dimensions of the cylindrical shell are 400 mm in diameter, 500 mm in height and 8 mm in wall thickness, and the material is Q235 steel. The load characteristics are as follows:

- Load action direction: inward along the outer normal direction.
- Time-domain distribution: rectangular pulse with a pulse duration of 5 ms in the range of ±0.5° and 10 ms in the range of 89.5° to 90.5°.
- The load amplitude distribution is as follows:

(a) Load 1:

$$P(r,\theta,z)=1+0.01z \text{ MPa}, \quad r=200 \text{ mm}, \quad -0.5°\leqslant\theta\leqslant 0.5° \tag{26}$$

That is to say, the structure is subjected to a pressure load increasing with the increase in *z*-direction within the range of ±0.5°.

(b) Load 2:

$$P(r,\theta,z)=2-0.02z \text{ MPa}, \quad r=200 \text{ mm}, \quad 89.5°\leqslant\theta\leqslant 90.5° \tag{27}$$

In other words, the structure is subjected to a pressure load that decreases with an increase in *z*-direction within the range of 89.5° to 90.5°.

It is evident that Loads 1 and 2 do not have rotational similarity, however, by spatially dividing the load along the *z*-axis, as shown in Figure 6, the load has rotational similarity in each of the equally divided sections.

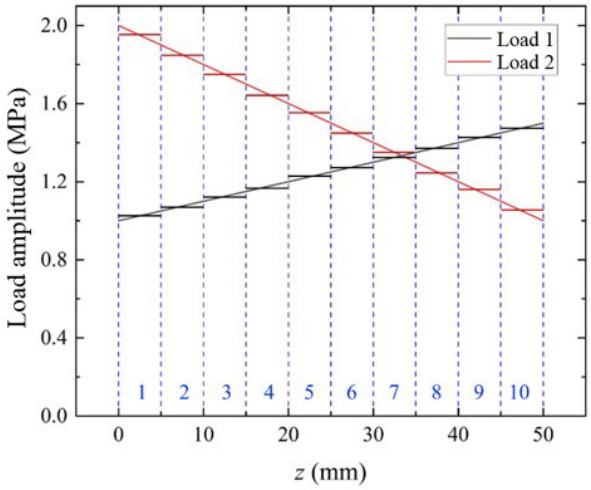


Figure 6. Schematic diagram of load division in space domain (*z*-direction).

3.1.2 Finite element modeling

Several finite element simulations of the mechanical responses of the cylindrical shell under the dynamic pressure loads were performed using the explicit finite element algorithm based on PANDA platform (Chen et al 2011). This study only involves linear elastic deformation, so in the finite element model, the material constitutive model is linear elastic, the material is Q235 steel (density: 7800 kg/m^3, elastic modulus: 210 GPa, Poisson's ratio: 0.3), and the contact, friction and material damping were not considered. A 4-node, quadrilateral, stress/displacement shell element with reduced integration. The bottom end of the cylindrical shell was clamped, and the two loads, Loads 1 and 2, were separately applied in two different calculations and simultaneously applied in a combined calculation. Besides, the time incrementation was calculated by an adaptive algorithm.

3.1.3 Finite element result analysis

The acceleration, velocity, and displacement responses at the top of the cylindrical shell structure at 180° were obtained using finite element calculations. Based on the finite element results of applying Load 1, the results of applying Loads 1 and 2 simultaneously were obtained using the generalized rotation-superposition method. In addition, the results obtained by the rotation-superposition method were compared with the direct finite element results of applying Loads 1 and 2 simultaneously, as shown in Figure 7. It can be seen from Figure 7 that the results of the two methods are in good agreement, indicating that the generalized rotation-superposition method is accurate and reliable for problems with complex spatio-temporal load distributions.

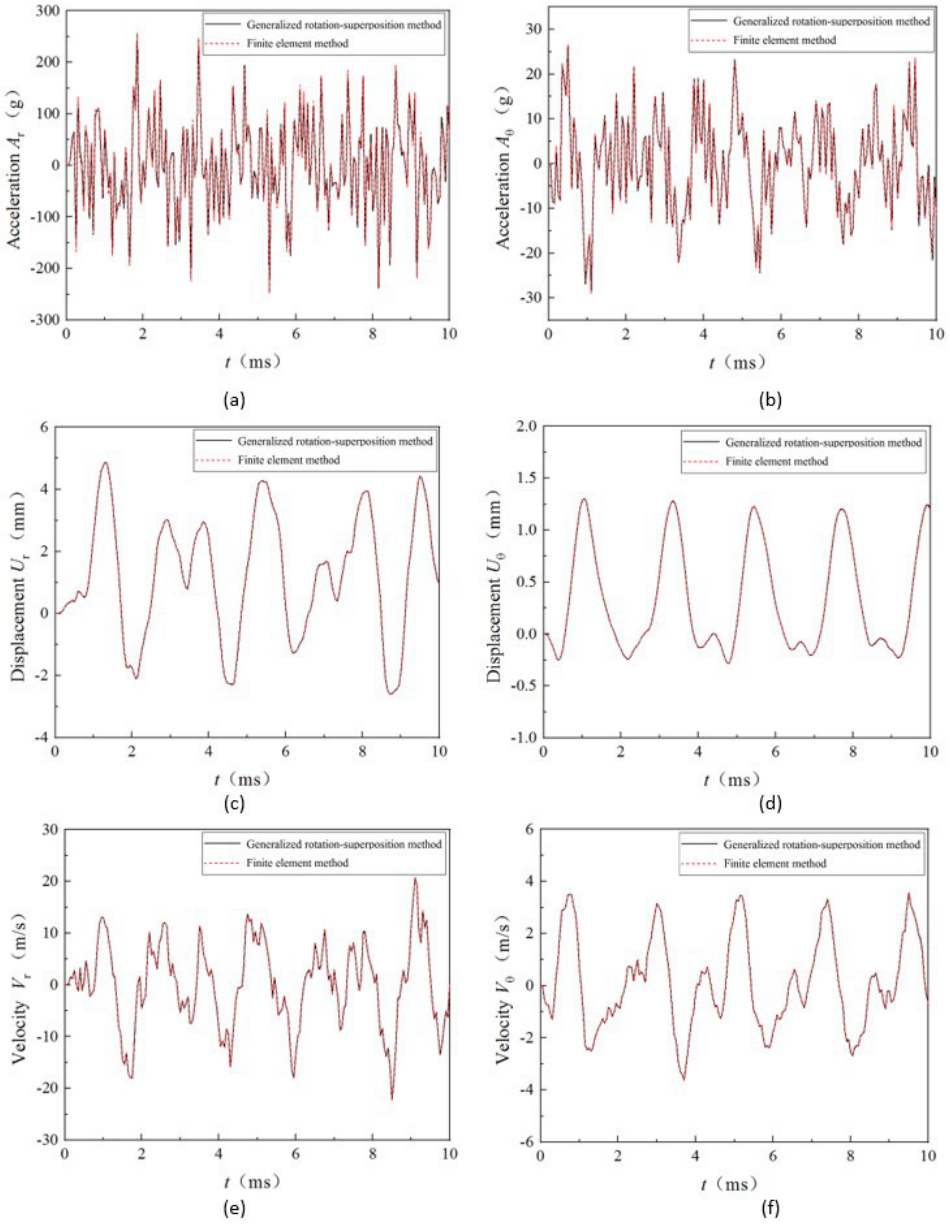


Figure 7. Comparison of the results by two methods. (a) radial acceleration A_{r}; (b) circumferential acceleration A_{θ}; (c) radial displacement U_{r}; (d) circumferential displacement U_{θ}; (e) radial velocity V_{r}; (f) circumferential velocity V_{θ}.

3.2 For generalized rotationally symmetric structures

3.2.1 Problem description

Assuming that the corrugated sandwich cylindrical shell is subjected to a dynamic surface load, the geometric dimensions of the structure are as shown in Figure 8, where the height of the structure is $L = 500\ \mathrm{mm}$, the radius of the inner panel of the structure is $R_i = 160\ \mathrm{mm}$, the radius of the outer panel of the structure is $R_0 = 200\ \mathrm{mm}$, a

single corrugation corresponds to the central angle $\alpha = 20°$, and the wall thickness $t = 5$ mm. The loads are given as follows:

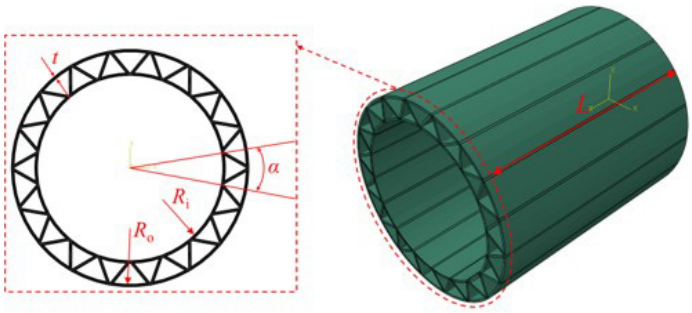


Figure 8. Geometric schematic diagram of the corrugated sandwich cylindrical shell.

- Load action direction: inward along the outer normal direction.
- Time-domain distribution: triangular pulse with pulse width of 10ms.
- The load amplitude distribution is expressed as follows:

(a) Load 3:

$$P(r,\theta,z) = 1 \text{ MPa}, \quad r = 200 \text{ mm}, \quad -1.43° \leqslant \theta \leqslant 1.43° \tag{28}$$

(b) Load 4:

$$P(r,\theta,z) = 1.5 \text{ MPa}, \quad r = 200 \text{ mm}, \quad 58.57° \leqslant \theta \leqslant 61.43° \tag{29}$$

(c) Load 5:

$$P(r,\theta,z) = 1.5 \text{ MPa}, \quad r = 200 \text{ mm}, \quad 88.57° \leqslant \theta \leqslant 91.43° \tag{30}$$

3.2.2 Finite element modeling

A few finite element simulations of the mechanical responses of the corrugated sandwich cylindrical shell under the dynamic pressures were performed. The finite element algorithm, material constitutive, meshing and boundary conditions of the finite element model were the same as those in Section 3.1.2. Load conditions include applying Load 3 alone, Loads 3 and 4 simultaneously, and Loads 3 and 5 simultaneously. Wherein, the rotation angle from Load 3 to Load 4 on the structure is an integer multiple of the axisymmetric period of the structure (i.e. $\Delta\theta = s\theta_0$), whereas, the angle between Load 3 and Load 5 is not an integer multiple of the symmetric period (i.e. $\Delta\theta \neq s\theta_0$).

3.2.3 Finite element result analysis

The acceleration, velocity and displacement responses at the top of the structure at 180° were obtained through finite element calculations. Based on the finite element results of applying Load 3, the results of applying Loads 3 and 4 simultaneously, and the results of applying Loads 3 and 5 simultaneously are obtained by the generalized rotation-superposition method. As an example, the acceleration results obtained by the generalized rotation-superposition method were compared with the direct finite element results, as shown in Figure 9.

It can be observed from Figures 9(a) and (b) that when $\Delta\theta = s\theta_0$, the results obtained by the generalized rotation-superposition method are in good agreement with the direct calculation results obtained by the finite element method. While, it can be seen from Figures 9(c) and (d) that when $\Delta\theta \neq s\theta_0$, the results obtained by the generalized rotation-superposition method are quite different from the results obtained directly by the finite element calculation. In summary, for generalized rotationally axisymmetric structures, the generalized rotation-superposition method is accurate and reliable only if the load is correctly divided and rotated, i.e., $\Delta\theta = s\theta_0$ must be insured.

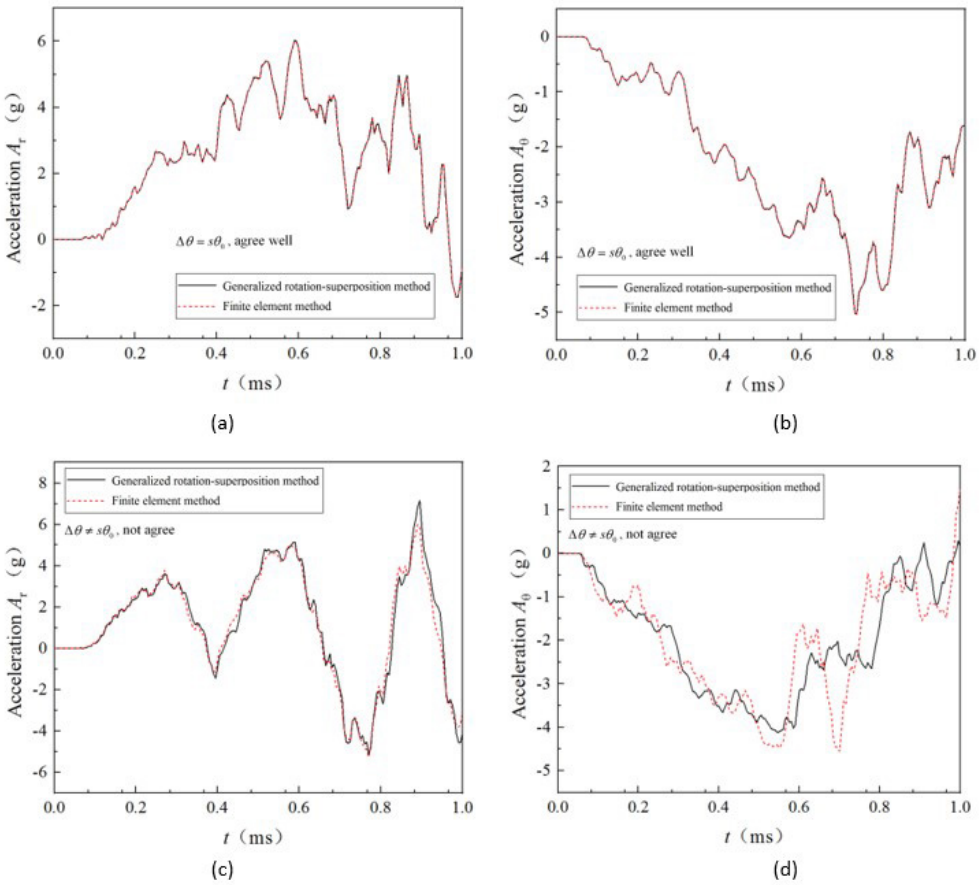


Figure 9. Geometric schematic diagram of the corrugated sandwich cylindrical shell. Comparison of the results of two methods. a)$\Delta\theta = s\theta_0$, radial acceleration A_r (agree well); b) $\Delta\theta = s\theta_0$, circumferential acceleration A_θ (agree well); c)$\Delta\theta \neq s\theta_0$, radial acceleration A_r (not agree); d) $\Delta\theta \neq s\theta_0$, circumferential acceleration A_θ (not agree).

4 APPLICATION AND DISCUSSION

A hyperbolic cooling tower under blast loads of near-field explosions is studied, as an example, to address the safety analysis problem of a typical engineering structure by the generalized rotation-superposition method. Any change in the explosive TNT equivalent (W), height of the explosion point from the ground (h), or distance from the explosion point to the axis of the tower (d) will lead to significant changes in the structural responses, as shown in Figure 10. To obtain the influences of the above parameters directly through finite element calculations, a large number of finite element models and calculations are required.

However, only a small number of finite element calculations are required using the generalized rotation-superposition method. Combined with the Conwep model (Guzas and Earls 2010), the structural response data for different W, different h and different d were obtained. This method can significantly improve the calculation efficiency, and the specific process is shown in Figure 11.

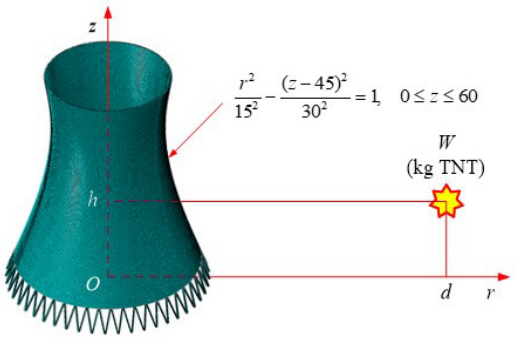


Figure 10. Sketch of the hyperbolic cooling tower subjected to near-field blast.

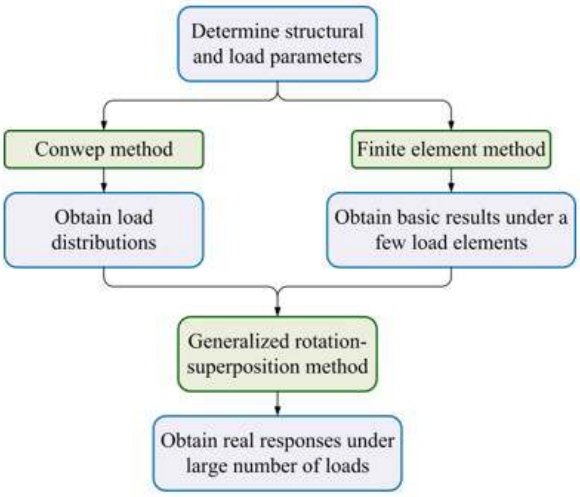


Figure 11. Flowchart for calculating the responses of the cooling tower under various working conditions using the generalized rotation-superposition method.

4.1 Structural parameters

The equation of the outer surface of the cooling tower is:

$$\frac{r^2}{15^2}-\frac{(z-45)^2}{30^2}=1,\quad 0\le z\le 60 \tag{31}$$

where, the structure with $h = 0-6$ m is the herringbone columns with a diameter of 0.6 m, a total of 48 pairs; the structure with $h = 6-6.5$ m is the bearing ring; the structure with $h = 6.5-60$ m is the tower body, and the thickness of the tower body is 0.5 m. The material of the cooling tower body is C30 concrete, the modulus of elasticity is 30 GPa, Poisson's ratio is 0.2, and the density is 2500 kg/m^3. The material of the herringbone columns and the bearing ring is C40 concrete, the modulus of elasticity is 32.5 GPa, Poisson's ratio is 0.2, and the density is 2500 kg/m^3.

4.2 Load distribution

Because of the small area of herringbone columns, the blast load they receive can be ignored in the actual calculation. According to the Conwep method (Guzas and Earls 2010), the expression of the pressure-time curve of each point on the cooling tower is:

$$P(\alpha,t)=P_{\mathrm{r}}(t)\cos^2\alpha+P_{\mathrm{s}}(t)(1+\cos^2\alpha-2\cos\alpha) \tag{32}$$

where P is the overpressure, α is the incident angle, t is the time, P_{r} is the reflected overpressure, and P_{s} is the incident overpressure. The function form of overpressure P with time t is:

$$P(t)=\begin{cases}0 & t<t_{\mathrm{a}}\\ P_{\max}\left(1-\dfrac{t-t_{\mathrm{a}}}{t_{\mathrm{d}}}\right)\mathrm{e}^{-b\left(1-\frac{t-t_{\mathrm{a}}}{t_{\mathrm{d}}}\right)}, & t_{\mathrm{a}}\le t\le t_{\mathrm{a}}+t_{\mathrm{d}}\\ 0 & t>t_{\mathrm{a}}+t_{\mathrm{d}}\end{cases} \tag{33}$$

where, $P_{\max}$ is the peak value of the overpressure, t_{a} is the load arrival time, t_{d} is the load delay time, and b is the load attenuation coefficient. The calculation formulas for P_{r}, P_{s}, t_{a}, t_{d}, and b can be found in the literature (Guzas and Earls 2010). One of the surface load distributions on the cooling tower calculated using the Conwep method is shown in Figure 12 as an example. It can be seen that the load is very complex because the pressure amplitude and the time-domain distribution both vary with the location on the outer surface of the cooling tower.

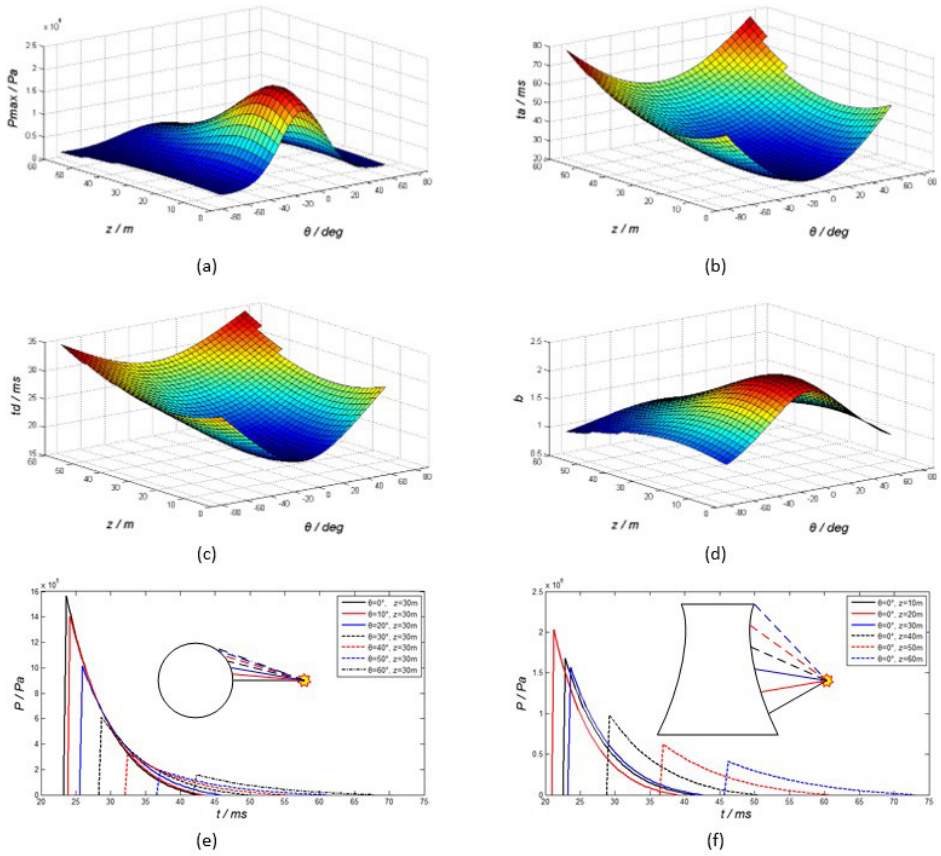


Figure 12. An example for near-field blast load on the surface of the cooling tower calculated by Conwep method. a) overpressure amplitude $P_{\max}$ varying with θ and z; b) arriving time t_{a} varying with θ and z; c) delay duration t_{d} varying with θ and z; d) decay coefficient b varying with θ and z; e) pressure histories with the same z and different θ; f) pressure histories with the same θ and different z.

4.3 Basic results by finite element calculations

According to the calculation flowchart shown in Figure 11, some basic result data under a few basic load elements are necessary and should be obtained through finite element calculations. In order to determine the basic load elements, we divided the structure into 48 parts (matching the 48 pairs of herringbone columns) in the circumferential direction and 10 parts in the axial direction, and applied 10 basic load elements in the 10 areas near 0°, respectively. The basic load elements are rectangular pressure waves in time domain, the time duration is 1 ms, and the pressure amplitude is 1 MPa. From top to bottom, they are named Load 1, Load 2, ..., Load 10, as shown in Figure 13. A total of 10 finite element calculations were performed to obtain corresponding mechanical response data under the 10 basic load elements.

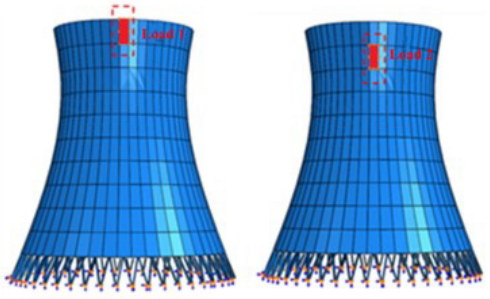


Figure 13. Schematic diagram of the basic load elements for basic finite element simulations.

4.4 Extended results by generalized rotation-superposition method

This example discusses the safety distances under different TNT equivalents at different heights and then plots the safety contour lines by fitting the dots (determined by the explosion heights and safety distances) for different TNT equivalents.

Therefore, after using the Conwep model to obtain the load distribution on the tower surface, a rotational similarity relationship between the real load and the basic load element can be established. According to the similarity relationship, based on the basic result data, the real structural response data can be obtained using the generalized rotation-superposition method. By the same way, the stress data of 10 points evenly distributed from top to bottom on the outer surface of the cooling tower at 0° (closest to the explosion point) under different W, different h and different d values were obtained. Further, the tensile strength of C30 concrete is 2.01 MPa as the safety judgment standard of the cooling tower, and finally the contour line of the spatial position of the explosion point was obtained when the maximum stress on the cooling tower reaches 2.01 MPa under different W (2000 kg to 20000 kg), as shown in the Figure 14. It can be seen from Figure 14 that, first, the safety contour lines are approximately parallel, and the more the TNT equivalent is, the nearer the line is to the tower. This agrees with our general understanding of the damage capability of explosions. Second, the safety contour lines appear sparse near the tower and compact far from it. The mechanism is that the shock wave overpressure of the explosion decays nonlinearly with the distance, and the farther from the explosion location, the faster it decays (Guzas and Earls 2010). Third, the safety contour lines change non-monotonically with the explosion height. This can be explained by the fact that the location (i.e. the height) of the maximum stress is not fixed but changes on the outer surface of the tower; therefore, the safety limits show complicated trends along the height direction for different TNT equivalents.

4.5 Discussion

4.5.1 On efficiency

As for the computing efficiency, traditionally, to obtain the position of the explosion point when the cooling tower stress reaches 2.01 MPa in the same space domain under a certain TNT equivalent only directly through finite element calculations, it is necessary to carry out finite element calculations for the corresponding positions of all the red points as shown in Figure 15, with a total of 266 points. To further obtain the results under 10 different TNT equivalents, 2660 finite element calculations need to be carried out. However, in this study, only 10 basic finite element calculations were carried out using the generalized rotation-superposition method.

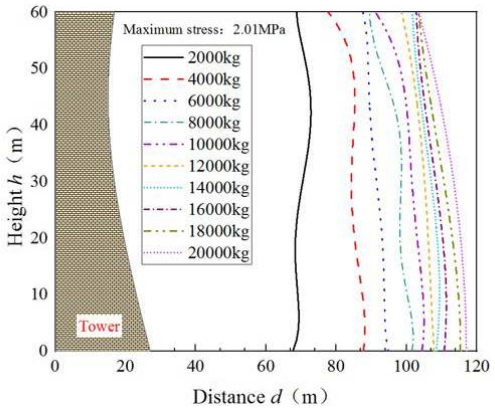


Figure 14. The safety contour lines (i.e. the safety limits) for different TNT equivalents calculated by the generalized rotation-superposition method based on 10 basic finite element simulations.

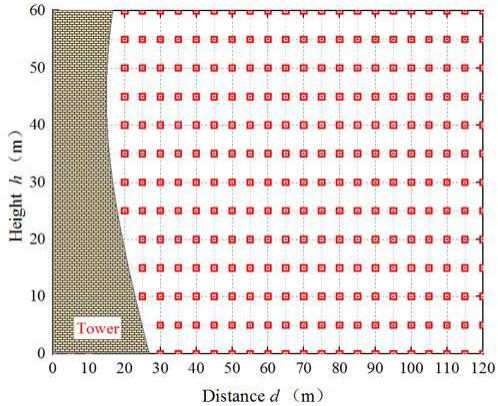


Figure 15. Number of numerical simulations by traditional finite element method, where there are 266 points for different distances and heights, and totally 2660 finite element simulations considering 10 TNT equivalents at each point.

According to the statistics of computing time (here only the computing time is considered and the handing time for modeling, data processing, etc., is ignored) using single-core personal computers, the time for a single finite element simulation (TFE) is 6.5 min approximately, and the time for a single arithmetic calculation using the generalized rotation-superposition method (TRS) is 0.096 min on average. Thus, if the factor of efficiency improvement (FEI) is defined as the ratio of the computing time for direct finite element simulations of all the working conditions to that for 10 basic finite element simulations plus necessary arithmetic calculations by the generalized rotation-superposition method, i.e. $FEI = NWC \cdot TFE \,/\, (10 \cdot TFE + NWC \cdot TRS)$, where NWC represents the number of working conditions, the FEI values with different NWC and different TFE can be calculated as shown in Table 1. For comparison, the FEI values when TFE is assumed as 32.5 min (5 times of the real) and 65 min (10 times of the real) are given in the third and the forth columns, respectively. It can be observed in Table 1 that, firstly, FEI increases monotonously with NWC, and FEI is quite considerable when NWC reaches or exceeds several decades. For the real statistics in the above application, FEI reaches 53.97 when $NWC = 2660$. Therefore, the advantage of the generalized rotation-superposition method appears when NWC is a relative large number. Secondly, if TRS remains constant, the longer TFE is, the larger FEI is, and finally FEI converges to the value of $TFE \,/\, TRS$ when NWC trends to infinity. This indicates that the fast method is more suitable for complex problems in which TFE is very long. The above observations show that the generalized rotation-superposition method can greatly improve the computational efficiency, especially for analyzing a massive amount of working conditions and/or complex and time-consuming problems.

4.5.2 On accuracy

As for the basic rotation-superposition method, it is derived by the principle of superposition without discretization or approximation, thus it has hardly accuracy loss except arithmetical operation errors. As for the generalized rotation-superposition method, spatial and temporal discretizations are utilized for treating the loads with complex distribution in space domain and time domain, respectively, thus discretization errors are inevitably introduced into the calculations and it is necessary to analyze and validate the errors when using the method. Actually, the discretization in deriving the new method is very similar to the classical numerical methods such as the finite element method. Therefore, error analysis and validation in applications can be performed in the similar ways in finite element method applications. Here some basic principles can be given as follows.

- The discretization density is locally determined by the variation rate of load distrubution, either in space domain or in time domain; and the higher the rate is, the denser the discretization should be.
- The discretization density distribution should be proper because there needs a balance between accuracy and efficiency.
- A proper discretization density distribution can be found when the computed results of structural responses do not evidently change with refining the meshes.
- The above “evident change” can be determined by the detailed computation requirements, for example, 5% can be generally considered.

4.5.3 On limitations

According to the derivation of the generalized rotation-superposition method, its limitations can be restated as follows.

- The structure must be generalized rotationally axisymmetric, in other words, it should be axisymmetric (such as cylinders and cones) or periodically axisymmetric (such as fans, gears, and corrugated sandwich shells).
- The problem must be linear, i.e., the nonlinear factors introduced from material constitution, geometric deformation, contact, friction, and so on, do not appear in loading and responding.
- The calculated responses must be vectors in cylindrical coordinate systems, such as displacement, velocity, acceleration, stress, and strain. The scalar quantities, such as energy and temperature, cannot be computed by the generalized rotation-superposition method.

Table 1. FEI values with different NWC and different TFE, where $TRS = 0.096$ min.

NWC	FEI		
	$TFE = 6.5$ min	$TFE = 32.5$ min	$TFE = 65$ min
0	0.00	0.00	0.00
1	0.10	0.10	0.10
2	0.20	0.20	0.20
3	0.30	0.30	0.30
4	0.40	0.40	0.40
5	0.50	0.50	0.50
6	0.59	0.60	0.60
7	0.69	0.70	0.70
8	0.79	0.80	0.80
9	0.89	0.90	0.90
10	0.99	1.00	1.00
20	1.94	1.99	1.99
30	2.87	2.97	2.99
40	3.78	3.95	3.98
50	4.66	4.93	4.96
60	5.51	5.90	5.95
70	6.34	6.86	6.93
80	7.15	7.82	7.91
90	7.94	8.77	8.88
100	8.71	9.71	9.85
200	15.44	18.88	19.43
300	20.79	27.56	28.73
400	25.15	35.77	37.77
500	28.76	43.57	46.56
600	31.81	50.97	55.12
700	34.42	58.01	63.44
800	36.67	64.71	71.55
900	38.64	71.10	79.44
1000	40.37	77.20	87.13
2000	50.58	125.73	154.39
2660	53.97	148.96	190.97
3000	55.24	159.05	207.89
4000	57.91	183.36	251.45
5000	59.63	201.86	287.61
6000	60.84	216.43	318.11
7000	61.74	228.18	344.18
8000	62.42	237.88	366.71
9000	62.97	246.01	386.39
10000	63.41	252.92	403.73
20000	65.49	289.53	505.84
30000	66.21	304.21	552.41
40000	66.58	312.12	579.06
50000	66.80	317.07	596.33
60000	66.95	320.46	608.42
70000	67.06	322.92	617.37
80000	67.14	324.80	624.25
90000	67.20	326.27	629.71
100000	67.25	327.46	634.15
∞ $(FEI = TFE / TRS)$	67.71	338.54	677.08

5 CONCUSION AND FURTHER WORK

Aiming at the problem that the application scope is limited by the rotational similarity of load and the structural axisymmetry, the basic rotation-superposition method was improved, and a fast algorithm for calculating the linear elastic responses of generalized rotationally axisymmetric structures under arbitrary mechanical loads was established, which is named generalized rotation-superposition method. The effectiveness and accuracy of the theoretical model

were proven by finite element simulations. For a complex application example, a hyperbolic cooling tower with decades of pairs of herringbone columns and a bearing ring subjected to near-field explosion loads was analyzed. Massive data of the structural responses of the cooling tower under 2660 different explosion loads were obtained using the generalized rotation-superposition method, and the safety contour lines under different TNT equivalents were obtained. This application case illustrates the applicability of the new method to complex engineering problems and the advantages of efficient acquisition of massive data. The proposed method can bridge numerical simulations and surrogate models, and further improve the computation efficiencies and precisions for a specific class of structural response problems in the traditional applications and the emerging digital twin applications.

5.1 Conclusions

Based on the above results and discussion, the following conclusions can be drawn:

- The new algorithm has high efficiency and high precision. Firstly, it can give massive structural results under a great number of working conditions only by arithmetic operations based on a small quantity of basic numerical results, thus the efficiency is very high. The above application shows that the factor of efficiency improvement reaches 53.97 for 2660 working conditions. Secondly, the algorithm is purely physics-based and is different from the data-driving methods such as surrogate models, so the precision is relatively high besides the errors from arithmetic operations and the necessary discretizations.
- The new algorithm is suitable for enhancing the combination of numerical methods and surrogate models, especially in digital twin applications. Due to its high efficiency and high precision, the new method can supply massive results on the basis of basic numerical results, helping surrogate models to improve their precisions.. This advantage is very useful in the emerging digital twin applications for online monitoring, analyzing, and predicting the structural status or performance.
- The new algorithm has less limitations compared to the early edition. It greatly expands the applicable scope, form rotationally similar loads to arbitrary loads, and from axisymmetric structures to generalized rotationally axisymmetric structures (including purely axisymmetric structures and periodically axisymmetric structures), consequently, there are less limitations.
- In addition, a basic understanding of safety contour lines of a hyperbolic cooling tower under blast loads of near-field explosions was obtained, and their characteristics can be summarized as follows:

  (a) The safety contour lines are approximately parallel.
  (b) The greater the TNT equivalent is, the farther the safety line is from the tower.
  (c) The closer to the tower, the sparser the safety contour lines scatter.
  (d) The safety contour lines change non-monotonically with the explosion height.

5.2 Further work

This study built the framework of the generalized rotation-superposition method. But for more practical applications in the traditional and the emerging fields, there are two aspects of further work to be done.

- Firstly, a friendly automatic software needs to be designed and implemented. The functions of the software should, at least, include automatic load analysis & processing and response computation.
- Additionally, a quantitative error estimation algorithm needs to be formulated. This algorithm can be embedded in the main software and conveniently help the users performing online model validation and improvement.

ACKNOWLEDGEMENTS

This study was supported by the National Natural Science Foundation of China (grant number 12072334).

Author's Contributions: Conceptualization, YJ Mao; Methodology, YJ Mao, M Yang and J Zhang; Investigation, M Yang and J Zhang; Writing, M Yang, H Chen, JL Yang and YJ Mao; Supervision, YJ Mao.

Editor: Rogério José Marczak

References

Addisu, H.S., Koricho, E.G. (2022). Structural weight and stiffness optimization of a midibus using the reinforcement and response surface optimization (RSO) method in static condition. Modelling and Simulation in Engineering 2022: 6812744.

Alizadeh, R., Allen, J.K., Mistree, F. (2020). Managing computational complexity using surrogate models: a critical review. Research in Engineering Design 31(3): 275-298.

Chen, C.J., Liu, Y., Zhang, Y.Z., Bai, X.Y., He, Y.B. (2011). Programming of parallel explicit finite element based on PANDA (in Chinese). Chinese Journal of Computational Mechanics 28(Suppl. 1): 204-207, 214.

Chen, G.D., Zhang, K., Xue, X.M., Zhang, L.M., Yao, C.J., Wang, J., Yao, J. (2022). A radial basis function surrogate model assisted evolutionary algorithm for high-dimensional expensive optimization problems. Applied Soft Computing 116: 108353.

Feng, N., Zhang, G.D., Khandelwal, K. (2022). Finite strain FE_2 analysis with data-driven homogenization using deep neural networks. Computers & Structures 263: 106742.

Feng, S., Hao, P., Liu, H., Du, K., Wang, B., Li, G. (2022). A data-driven Kriging model based on adversarial learning for reliability assessment. Structural and Multidisciplinary Optimization 65: 27.

Funk, S., Basmaji, A.A., Nackenhorst, U. (2023). Globally supported surrogate model based on support vector regression for nonlinear structural engineering applications. Archive of Applied Mechanics; 93(2): 825-839.

Guo, H.W., Zhuang, X.Y., Rabczuk, T. (2019). A deep collocation method for the bending analysis of Kirchhoff plate. Computers, Materials and Continua 59(2): 433-456.

Guo, M., Manzoni, A., Amendt, M., Conti, P., Hesthaven, J.S. (2022). Multi-fidelity regression using artificial neural networks: efficient approximation of parameter-dependent output quantities. Computer Methods in Applied Mechanics and Engineering 389(1): 114378.

Guo, Q., Wang, S.A. (2020). Free vibration analysis and optimal design of adhesively bonded double-strap joints by using artificial neural networks. Latin American Journal of Solids and Structures 17(4): e27

Guzas, E.L., Earls, C.J. (2010). Air blast load generation for simulating structural response. Steel and Composite Structures 10(5): 429-455.

He, W.B., Mao, J.X., Song, K., Li, Z., Su, Y.L., Wang, Y.N., Pan, X.C. (2022). Structural performance prediction based on the digital twin model: a battery bracket example. Reliability Engineering & System Safety 229(1): 108874.

Hu, Y., Guo, W., Long, Y., Li, S., Xu, Z.A. (2022). Physics-informed deep neural networks for simulating S-shaped steel dampers. Computers & Structures 267: 106798.

Ismail, M.S., Baharudin, B.T.H.T., Yahya, S.A., Kahar, H.A. (2013). Finite element analysis of composite cylinder with centre cutout under axial load and internal pressure. Advanced Materials Research 701: 425-429.

Ismail, M.S., Ifayefunmi, O., Fadzullah, S.H.S.M. (2020). Buckling analysis of stiffened cone-cylinder intersection subjected to external pressure. Key Engineering Materials 833: 223-227.

Ismail, M.S., Purbolaksono, J., Andriyana, A., Tan, C.J., Muhammad, N. Liew, H.L. (2015). The use of initial imperfection approach in design process and buckling failure evaluation of axially compressed composite cylindrical shells. Engineering Failure Analysis 51: 20-28.

Jin, S.S., Jung, H.J. (2016). Sequential surrogate modeling for efficient finite element model updating. Computers and Structures 168: 30-45.

Kabasi, S., Roy, A., Chakraborty, S. (2021). A generalized moving least square–based response surface method for efficient reliability analysis of structure. Structural Multidisciplinary Optimization 63(3): 1085-1097.

Keshtegar, B., Seghier, M.E.A.B., Zio, E., Correia, J.A.F.O., Zhu, S.P., Trung, N.T. (2021). Novel efficient method for structural reliability analysis using hybrid nonlinear conjugate map-based support vector regression. Computer Methods in Applied Mechanics and Engineering 381: 113818.

Koocheki, K., Pietruszczak, S. (2023). Numerical analysis of large masonry structures: bridging meso and macro scales via artificial neural networks. Computers & Structures 282: 107042.

Kudela, K., Matousek, R. (2022). Recent advances and applications of surrogate models for finite element method computations: a review. Soft Computing 26(24): 13709-13733.

Lai, X,N, He, X.W., Wang, S., Wang, X.B., Sun, W., Song, X.G. (2022). Building a lightweight digital twin of a crane boom for structural safety monitoring based on a multifidelity surrogate model. Journal of Mechanical Design 144(6): 064502.

Lai, X.N., He, X.W., Pang, Y., Zhang, F., Zhou, D.C., Sun, W., Song, X.G. (2023). A scalable digital twin framework based on a novel adaptive ensemble surrogate model. Journal of Mechanical Design 145(2): 021701.

Laplante, P. (2022). Trusting digital twins. Computer 55(7): 73–77.

Mahmoodzadeh, A., Nejati, H.R., Mohammadi, M., Ibrahim, H.H., Khishe, M., Rashidi, S., Ali, H.F.H. (2022). Prediction of Mode-I rock fracture toughness using support vector regression with metaheuristic optimization algorithms. Engineering Fracture Mechanics 264: 108334.

Mao, Y.J., Li, Y.L., Deng, H.J., Huang, H.J. (2010). A quick method for analyzing dynamic responses of axisymmetric structures under lateral impulsive loadings (in Chinese). Chinese Journal of Computational Mechanics 27(3): 563-568.

Mao, Y.J., Li, Y.L., Huang, H.J., Deng, H.J. (2011a). A quick method for solving responses of axisymmetric structures subjected to loads of rotational similarity: rotation-superposition method and its application (in Chinese). Chinese Journal of Solid Mechanics 32(3): 306-312.

Mao, Y.J., Li, Y.L., Huang, H.J., Wang, J.P. (2011b). Fast simulation of pyroshock responses of a conical structure using rotation-superposition method. Applied Mathematics & Information Sciences 5(2): 185S-193S.

Mao, Y.J., Wang, J.P., Zhou, Q., Huang, H.Y., Deng, H.J. (2019). Experimental Simulation Techniques of Structural Responses Induced by Intense Pulsed X-rays (in Chinese), Science Press.

Nakamura, N. (2012). Basic study on the transform method of frequency-dependent functions into time domain: relation to Duhamel's Integral and time-domain-transfer function. Journal of Engineering Mechanics 138(3): 276-285.

Norman, M.A.M., Razean, M.R.M., Rosaidi, M.H.M., Ismail, M.S., Mahmud, J. (2023). Effect of fibre volume on the natural frequencies of laminated composite plate. Materials Today: Proceedings 75: 133-139.

Pang, Y., Wang, Y.T., Lai, X.N., Zhang, S., Liang, P.W., Song, X.G. (2023). Enhanced Kriging leave-one-out cross-validation in improving model estimation and optimization. Computer Methods in Applied Mechanics and Engineering 414: 116194.

Samaniego, E., Anitescu, C., Goswami, S., Nguyen-Thanh, V.M., Guo, H., Hamdia, K., Zhuang, X., Rabczuk, T. (2020). An energy approach to the solution of partial differential equations in computational mechanics via machine learning: Concepts, implementation and applications. Computer Methods in Applied Mechanics and Engineering 362: 112790.

Santana, P.B., Gomes, H.M., Ferreira, A.M., Tita, V. (2023). A multiobjective optimization framework for strength and stress concentration in variable axial composite shells: a metaheuristic approach. Latin American Journal of Solids and Structures 20(6): e497

Stoffel, M., Gulakala, R., Bamer, F., Markert, B. (2020). Artificial neural networks in structural dynamics: A new modular radial basis function approach vs. convolutional and feedforward topologies. Computer Methods in Applied Mechanics and Engineering 364: 112989.

Teng D., Feng, Y.W., Chen, J.Y. (2022). Intelligent moving extremum weighted surrogate modeling framework for dynamic reliability estimation of complex structures. Engineering Failure Analysis 138: 106364.

Tiemoshenko, S.P., Goodier, J.N. (2004). Theory of Elasticity (Third Edition), McGraw-Hill Education (Asia) Co. and Tsinghua University Press.

Wang, L., Liu, Y.R., Gu, K.X., Wu, T. (2020). A radial basis function artificial neural network (RBF ANN) based method for uncertain distributed force reconstruction considering signal noises and material dispersion. Computer Methods in Applied Mechanics and Engineering; 364: 112954.

Wang, Y.J., Pan, H., Shi, Y.N., Wang, R.L., Wang, P. (2023). A new active-learning estimation method for the failure probability of structural reliability based on Kriging model and simple penalty function. Computer Methods in Applied Mechanics and Engineering 410: 116035.

Yang, K., Chen, Y.W., Wang, Y.B., Chen, H., Wang, S.R. (2023). Analysis and optimization of impact energy absorption performance of mine refuge chamber filled with concave triangular negative poisson's ratio material. Latin American Journal of Solids and Structures 20(3): e483.

Yang, M., Han, B., Mao, Y.J., Zhang, J., Lu, T.J. (2022). Crashworthiness of foam filled truncated conical sandwich shells with corrugated cores. Thin-Walled Structures 179: 109677.

Yang, M., Han, B., Su, P.B., Li, F.H., Zhao, Z.N., Zhang, Q., Zhang, Q.C., Hong, Z.J., Lu, T.J. (2021a). Oblique crushing of truncated conical sandwich shell with corrugated core. Mechanics of Advanced Materials and Structures 28(23): 2458-2471.

Yang, M., Han, B., Su, P.B., Zhang, Q., Zhang, Q.C., Zhao, Z.Y., Ni, C.Y., Lu, T.J. (2021b).Crashworthiness of hierarchical truncated conical shells with corrugated cores. International Journal of Mechanical Sciences 193: 106171.

Zhou, T., Peng, Y.B. (2023). An active-learning reliability method based on support vector regression and cross validation. Computers & Structures 276: 106943.

Zhuang, X.Y., Guo, H.W., Alajlan, N., Zhu, H.H., Rabczuk, T. (2021). Deep autoencoder based energy method for the bending, vibration, and buckling analysis of Kirchhoff plates with transfer learning. European Journal of Mechanics - A/Solids 87: 104225.